HAL open science

New superhard tetragonal BCN from crystal chemistry and first principles

Samir Matar, Vladimir Solozhenko

To cite this version:

Samir Matar, Vladimir Solozhenko. New superhard tetragonal BCN from crystal chemistry and first principles. Materialia, 2022, 26, pp.101581. 10.1016/j.mtla.2022.101581 . hal-03788871

HAL Id: hal-03788871

https://hal.science/hal-03788871v1

Submitted on 27 Sep 2022

HAL is a multi-disciplinary open access archive for the deposit and dissemination of scientific research documents, whether they are published or not. The documents may come from teaching and research institutions in France or abroad, or from public or private research centers.

L'archive ouverte pluridisciplinaire **HAL**, est destinée au dépôt et à la diffusion de documents scientifiques de niveau recherche, publiés ou non, émanant des établissements d'enseignement et de recherche français ou étrangers, des laboratoires publics ou privés.

New superhard tetragonal BCN from crystal chemistry and first principles

Samir F. Matar [1] and Vladimir L. Solozhenko [2,*]

[1] Lebanese German University (LGU), Sahel Alma, Jounieh, Lebanon
https://orcid.org/0000-0001-5419-358X

[2] LSPM–CNRS, Université Sorbonne Paris Nord, 93430 Villetaneuse, France
https://orcid.org/0000-0002-0881-9761

Abstract:

Novel ternary equiatomic BCN compound structurally based on the 'glitter' C_6 with both tetrahedral (sp^3) and trigonal (sp^2) carbons has been predicted using crystal chemistry rationale and supported by first principles calculations of energies and energy dependent quantities within density functional theory (DFT). Crystal structure of BCN belongs to the tetragonal space group $P4_2mc$ and is built by stacking of corner sharing BC_2N_2 tetrahedra. The phase is found energetically cohesive and stable both mechanically (elastic properties) and dynamically (phonons band structures). The electronic band structures reveal metallic-like behavior. Characterized by very high Vickers hardness (65 GPa), BCN is expected to be a prospective superabrasive.

Keywords: Tetragonal BCN; DFT; elastic constants; hardness; anisotropy; phonon dispersion; electronic band structure.

[*] Corresponding author (vladimir.solozhenko@univ-paris13.fr)

1- Introduction

In 2001, cubic boron carbonitride of BC_2N composition (c-BC_2N) was synthesized at high pressure – high temperature conditions [1]. The new phase possesses Vickers hardness of 76 GPa [2] which make it the second after diamond hardest material. At ambient pressure in an inert atmosphere c-BC_2N remains stable up to 1800 K, and, thus, is characterized by significantly higher thermal stability than polycrystalline diamond.

A year later, superhard low-compressible cubic BN-C solid solutions with stoichiometry close to BCN (so-called c-BCN) were synthesized by isoentropic shock compression [3]. According to TEM-SAED-EELS studies [4], boron, carbon and nitrogen atoms are homogeneously distributed over c-BCN crystal lattice without forming superstructures. c-BCN has one of the largest bulk modulus (B_0 = 412 GPa [3]) being second only to diamond, and very high Knoop hardness (52 GPa [5]).

Ternary B–C–N phases of various stoichiometries (monoclinic BCN [6], orthorhombic [7] and rhombohedral [8] BC_2N, tetragonal and rhombohedral BC_6N [9], monoclinic BC_8N [10], etc.) have been predicted from first-principles studies, but none of them have been synthesized so far.

In the present paper a new tetragonal equiatomic boron carbonitride is proposed from crystal chemistry rationale and *ab initio* calculations within DFT [11]. The proposed BCN structure is identified with higher symmetry than monoclinic BCN [6], and a local tetrahedral configuration favoring *BC2N2* tetrahedra over *NB2C2* ones. Tetragonal BCN is found cohesive and characterized as mechanically and dynamically stable, with exceptional hardness properties.

2- Computational framework

The search for the ground state energy structures is required to distinguish between stable and unstable phases before further investigation. In the DFT framework we used the Vienna Ab initio Simulation Package (VASP) code [12-14] with the projector augmented wave (PAW) method [13,14] for the atomic potentials. The exchange-correlation XC effects were considered using the generalized gradient approximation (GGA) [15].

For the relaxation of the atoms onto ground state geometry, a conjugate-gradient algorithm [16] was applied. Improved tetrahedron method [17] with corrections according to Methfessel-Paxton scheme [18] was used for geometry optimization and energy calculations. A special **k**-point sampling [19] was applied for approximating the reciprocal space Brillouin-zone (BZ) integrals. For better reliability, the optimization of the structural parameters was carried out along with successive self-consistent cycles with increasing mesh until the forces on atoms were less than 0.02 eV/Å and the stress components below 0.003 eV/Å^3.

Besides the elastic constants calculated to evaluate the mechanical stability and hardness, further calculations of phonon dispersion curves were carried out to verify the dynamic stability. In the present work, the phonon modes were computed considering the harmonic approximation via finite displacements of the atoms around their equilibrium positions to obtain the forces from the summation over the different configurations. The phonon dispersion curves along the direction of the Brillouin zone were subsequently obtained using the "Phonopy" interface code based on the Python language [20].

Finally, the electronic band structures and the site projected density of states (DOS) were obtained with full potential Augmented Spherical Wave (ASW) method [21].

3- Crystal chemistry considerations and pertaining cohesive properties

CN-containing compounds are generally called 'cyanides'(CN^- anion) such as NaCN [22] and $Al(CN)_3$ [23] while 'cyanamides' correspond to CN_2^{2-} anion. Regarding the first element in IIIA group, boron is labeled as a *metalloid*, i.e. half-way between metal and non-metal. Boron combination with nitrogen leads to the binary compound BN called boron nitride, implying trivalent boron with "$B^{3+}N^{3-}$" ionic-like chemical formulation. However, BN is rather *polar covalent* as it can be inferred from the Pauling electronegativity differences ($\Delta\chi$). Considering the average electronegativity of CN: $<\chi(CN)> = (2.55+3.44)/2 \sim |3.0|$, NaCN has $\Delta\chi = 0.9–3.0 = |2.1|$, whereas BN is characterized by $\Delta\chi = 2.04–3.44 = |1.4|$. For presently proposed BCN $\Delta\chi = 2.04–3.0 = |0.96|$ which indicates a decrease of ionic character in the NaCN–BN–BCN row. The ternary equiatomic BCN can be considered as a carbonitride where B is equally connected to C and N within the *BC2N2* tetrahedra. Other possible configurations are octahedral, square planar or linear; the cohesive energy criterion will allow distinguishing them.

a) Preliminary calculations considering different local coordinations for boron

As template structures, first we considered CoCN [24], NaCN [22] and CuCN [25] involving octahedral, square-planar, and linear coordinations for the metal, respectively. The tetrahedral coordination is considered in the next sub-section.

Full geometry optimization calculations led to the BCN structures shown in Fig. 1 (a, b, c). The respective local boron coordinations announced above for the template structures are confirmed for the BCN models. The upper part of Table 1 provides crystal symmetry and computed energies for all three BCN models. The atom-averaged cohesive energies were obtained after subtracting the atomic energies given in the last line of Table 1. The most favorable structure is the orthorhombic one presenting square planar *BC2N2* coordination (Fig. 1b), and the least favorable is CoCN-type structure where B is hexacoordinated with *BC3N3*-like octahedron shown in Fig. 1a, that is clearly excluded for boron. Linear B-C-N

local arrangements in the CuCN-like BCN (Fig. 1c) lead to an intermediate energy situation. Lastly, $Al(CN)_3$ [23] was considered to propose possible $B(CN)_3$ for the sake of verifying the valence hypothesis since Al is trivalent and belongs to IIIA group. The resulting cohesive energy of -1.341 eV, within range of the CuCN-type BCN (Table 1) indicates a non-favorable structure, thus confirming that BCN is not a 'cyanide'.

b) Ground state solution for BCN

Despite the relative stability of layered orthorhombic BCN, which is the first proposition of layered-like structure in the B-C-N ternary system, it remains a non-compact 2D-like structure. A template 3D model allowing a tetrahedral coordination for B with N and C and connected *BC2N2* tetrahedra was needed. The crystal structure of hexacarbon C_6 proposed in 1994 [26] (Fig. 2a) has the unique characteristics of possessing two different types of carbon: tetrahedral C1 and trigonal C2, the latter forming C2-C2 pairs that separate the $C1C2_4$ tetrahedra. C_6 is consequently expressed as $C1_2C2_4$. The replacement of C1 by B leads to hypothetic boron dicarbide B_2C_4 (Fig. 1b) which shows the same tetrahedral stacking as in C_6. Both structures are defined in tetragonal space group $P4_2/mmc$ (cf. Tables 1 & 2).

Turning to the ternary BCN compound, since two C2 belong to the same Wyckoff site (4*i*) the replacement of one carbon by nitrogen leads to $B_2C_2N_2$ (or BCN) where B is tetrahedral (sp^3-like), and N and C occupy the C trigonal sites. The initial tetragonal space group $P4_2/mmc$ (N°131) symmetry is consequently lowered, and subsequent crystal structure determinations after geometry relaxation led to define the ternary phase in a new space group $P4_2mc$ (N°105) (Fig. 2c), i.e. with the loss of a mirror (*m*) symmetry due to the occupation of the fourfold (4*i*) ½, 0, *z* position in B_2C_4 (Table 2b) by two different atoms, N and C, which are now are in twofold (2c) ½, 0, *z* positions (Table 2c). The interatomic distances show almost unchanged d(C2-C2) = 1.34–1.35 Å in both C_6 and B_2C_4, but the replacement of one C by N leads to the shorter d(C-N) = 1.29 Å arising from a larger charge transfer C → N as depicted in next section on charge density trends. Within the tetrahedral site the replacement of C by larger size B leads to increase the distance in the binary phase and to differentiated d(B-C) > d(B-N) in the ternary phase. The resulting effect on the whole structure of the ternary phase is a slightly smaller unit cell volume, i.e. a more compact compound, likely resulting in lower compressibility. Lastly, we examine the angle magnitudes. Tetrahedral ∠C2-C1-C2 = 106.795° in C_6 is smaller than 109.4°-value for ideal C(sp^3), and trigonal ∠C1-C2-C2 = 122.517° is slightly larger than the ideal 120°, resulting from the concurrent presence of two kinds of hybridization in the same structure. The angles change upon perturbing the structure further with B and N substitutions are shown in Table 2 (b, c).

Lastly, the *NB2C2* coordination in the structures proposed for BC_2N [7] was tested in the new space group $P4_2mc$ (N°105), i.e. by calculating $N(tetr.)_2B(trig.)_2C(trig.)_2$. The calculated

cohesive energy of ~ -0.95 eV/at. is clearly not favorable, and such tetrahedra in any B-C-N ternary phase should be minimized.

c) Cohesive energies

The energies presented in Table 1 show cohesive systems for hexacarbon, B_2C_4 and $B_2C_2N_2$ with magnitudes systematically larger than in the above examined structures. These results highlight the preference of boron for tetrahedral coordination. The largest cohesive system is the pseudo-unary C_6, characterized by small interatomic distances, and followed (unexpectedly) by the ternary phase with a small difference of 0.09 eV, explained by the presence of N that involves smaller distances compared to B_2C_4. Regarding formerly published BC_2N [7], the cohesive energies of the two orthorhombic phases are close and slightly larger (~0.18 eV/at.) than that of novel equiatomic BCN, whose stability validation is further provided based on elastic and dynamic properties in Section 4.

These observations are also illustrated with charge density projections revealing chemical behavior, on one hand, and from accurate analyses of the mechanical and dynamic stabilities characterizing all three C_6, B_2C_4, and $B_2C_2N_2$ phases, on the other hand.

d) Charge density projections

The *electronic-structure* ↔ *crystal-structure* relationship is presented by the charge density projections. Figure 3 panels show the charge density yellow volumes in the tetragonal phases C_6, B_2C_4 and $B_2C_2N_2$.

In C_6 (Fig. 3a) the charge density around C1 tetrahedral site shows sp^3-like yellow volumes, oppositely to trigonal C2 (sp^2-like) site exhibiting strong density in-between C2-C2 as illustrated by the red areas. This confirms the chemical behavior difference between carbons belonging to the two sites. Replacing C1 by less electronegative B ($\chi_C = 2.55 > \chi_B = 2.04$) leads to a large charge transfer from B to trigonal C (C2 in C_6). Due to this charge transfer, the C-C trigonal groups show a larger charge envelop versus C2-C2 in Fig. 3b. However, there can be observed skewed charge envelops of the four carbons around boron forming the *BC4* tetrahedra.

The replacement of one C2 by N, leading to equiatomic $B_2C_2N_2$, shows a differentiated charge envelop along the C-N pairs with the largest yellow charge volume around N (Fig. 3c). These results are chemically sound since they go along with the electronegativity trends: $\chi(N) = 3.04 > \chi(C) = 2.55 > \chi(B) = 2.04$, with subsequent trends of charge transfers δ: $\delta(N) = -2.66$, $\delta(C) = -0.28 > \delta(B) = +2.94$.

4- Mechanical properties and dynamic stability

a) Mechanical properties

(i) *Elastic constants*

The elastic constants C_{ij} required to derive the mechanical properties were determined by performing finite distortions of the lattice and obtaining C_{ij} from the strain-stress relationship. The bulk and shear moduli are usually obtained by averaging the single-crystal elastic constants using Voigt's method [27] based on a uniform strain. The calculated sets of elastic constants are given in Table 3. All values are positive, which is the first indication of mechanical stability. Further proofs were obtained from C_{ij} combinations obeying rules related to mechanical stability. The elastic constants C_{ij} and the mechanical stability for the tetragonal system are then described as follows:

$$C_{ii}\ (i = 1, 3, 4, 6) > 0;\ \ C_{11} > C_{12};\ C_{11} + C_{33} - 2C_{13} > 0;\ \text{and}\ 2C_{11} + C_{33} + 2C_{12} + 4C_{13} > 0.$$

The equations providing the bulk (B_V) and shear (G_V) moduli for the tetragonal system are as follows:

$$B_V = 1/9\ (2C_{11} + C_{33} + 2C_{12} + 4C_{13}).$$

$$G_V = 1/15\ (2C_{11} + C_{12} + 2\ C_{33} - 2C_{13} + 6C_{44} + 3C_{66})$$

Tetragonal 'glitter' C_6 has the highest elastic constants and the resulting bulk and shear moduli. Substituting B for C1 leading to B_2C_4 significantly reduces B_V and G_V, while the corresponding two moduli of $B_2C_2N_2$ show increase compared to B_2C_4 that can be explained by the shorter d(B-C) and d(B-N) of the ternary phase *versus* d(B-C) of the carbide (Table 2). Such results were further rationalized with the hardness calculation (see next sub-section).

(ii) *Hardness*

Vickers hardness (H_V) was predicted using three modern theoretical models: thermodynamic model based on crystal structure and thermodynamic properties [28]; Lyakhov-Oganov model which considers the strength of covalent bonding, degree of ionicity and topology of the crystal structure [29]; and empirical Chen-Niu model which uses elastic moduli (B and G) [30]. The fracture toughness (K_{Ic}) was evaluated within the Mazhnik-Oganov model [31], the only model that allows such predictions.

Table 4 presents Vickers hardness and other mechanical properties such as bulk (B), shear (G) and Young's (E) moduli, the Poisson's ratio (ν) and fracture toughness (K_{Ic}) of three new phases of the B-C-N system. One can see that H_V values obtained from thermodynamic and Lyakhov-Oganov models are in reasonable agreement, while hardness predicted by empirical Chen-Niu model is highly underestimated. As it was shown earlier [8,32], in the case of

superhard compounds of light elements thermodynamic model shows surprising agreement with available experimental data, and thus can be considered as the most reliable among all contemporary theoretical models of hardness.

The results obtained in the framework of the thermodynamic model of hardness show that 'glitter' C_6 has the highest hardness (83 GPa), which allows us to assign it to a family of ultra-hard materials [33]. Hardness of tetragonal BCN (65 GPa), although lower than those of cubic BC_2N [2] and diamond-like BN-C solid solutions [5], nevertheless exceeds the hardness of single-crystal cubic boron nitride (62 GPa [2]), so this new phase, if synthesized, could be a quite promising material especially considering its metallic-like behavior. Apparently, tetragonal equiatomic BCN can be synthesized only at extreme conditions in a rather narrow pressure-temperature range [34].

b) Dynamical stabilities from the phonons

Further stability criteria can be obtained from the phonon dispersion relations in the Brillouin zone, i.e. the phonon dispersions. Following the method presented in the 'Computational framework' section, the obtained phonon dispersion curves for C_6, B_2C_4 and $B_2C_2N_2$ are shown in Fig. 4. The bands span the main lines of the tetragonal BZ.

Along the vertical direction the frequency is given in units of terahertz (THz). There are 3N-3 optical modes at high energy, and 3 acoustic modes. The acoustic modes start from zero energy ($\omega = 0$) at the Γ point, center of the Brillouin zone, up to a few terahertz. They correspond to the lattice rigid translation modes of the crystal (two transverse and one longitudinal). While C_6 and $B_2C_2N_2$ present positive magnitudes of phonons, B_2C_4 shows negative magnitudes at Z point (see blue arrow) pointing to very soft modes that provide it with instability. Note that the replacement of carbon by nitrogen provides a dynamic stability to the ternary phase.

The remaining bands correspond to optic modes. In 'glitter' C_6 and $B_2C_2N_2$ (Figs. 4a and 4c) the highest bands are at 50 THz, i.e. the magnitude is higher than that in diamond ($\omega \approx 40$ THz according to Raman vibration spectroscopy [35]). Such high frequency is assigned respectively to the C2-C2 and C-N stretching. Thus, both phases are anisotropic as it already follows from their crystal structures.

5- Electronic band structures

The electronic band structures and the site projected density of states (DOS) are depicted in Figure 5. The energy along the vertical direction is with respect to the Fermi level E_F, and all three phases are metallic with bands crossing E_F. The different electronic behavior of tetrahedral C1 *versus* trigonal C2 can be observed from the DOS where vanishingly small

DOS are assigned to C1 whereas significant DOS are due to C2. These features are less obvious in the binary B_2C_4, but the ternary $B_2C_2N_2$ shows mixing N and C DOSs crossing E_F *versus* smaller contribution from boron tetrahedra.

6- Conclusions

This work focused on the identification of a valid structure of equiatomic boron carbonitride BCN devised from crystal chemistry rationalization of model structures submitted to unconstrained geometry optimization with DFT-based quantum mechanical calculations. Among different hypotheses, the most stable structure is based on *BC2N2* tetrahedra with a stacking resembling tetragonal 'glitter' C_6. Such BC_2N_2 tetrahedral arrangement seems to be preferable in the case of the ternary B-C-N phases. The energetic stability ensured from the cohesive energy was further confirmed for the mechanical and dynamic stabilities based on elastic constants and phonon band structures. Tetragonal BCN is a superhard phase that is harder than cubic boron nitride and possibly more thermally and chemically stable than diamond.

Conflicts of Interest: The authors declare no conflict of interest.

REFERENCES

[1] V.L. Solozhenko, D. Andrault, G. Fiquet, M. Mezouar, D.C. Rubie, Synthesis of superhard cubic BC_2N. *Appl. Phys. Lett.* **78** (2001) 1385-1387.

[2] V.L. Solozhenko, S.N. Dub, N.V. Novikov, Mechanical properties of cubic BC_2N, a new superhard phase. *Diam. Relat. Mater.* **10** (2001) 2228-2231.

[3] V.L. Solozhenko, Synthesis of novel superhard phases in the B-C-N system. *High Press. Res.* **22** (2002) 519-524.

[4] F. Langenhorst, V.L. Solozhenko, ATEM-EELS study of new diamond-like phases of the B-C-N system. *Phys. Chem. Chem. Phys.* **4** (2002) 5183-5188.

[5] V.L. Solozhenko, High-pressure synthesis of novel superhard phases. in: "*Comprehensive Hard Materials*" (eds. V.K. Sarin and C.E. Nebel), Elsevier, 2014, pp. 641-652.

[6] Z. Ma, C. Tang, C. Shi, A new BCN compound with monoclinic symmetry: First-principle calculations. *Materials* **15** (2022) 3186.

[7] M. Mattesini, S.F. Matar, Search for ultra-hard materials: theoretical characterization of novel orthorhombic BC_2N crystals. *Int. J. Inorg. Mater.* **3** (2001) 943–957.

[8] S.F. Matar, V.L. Solozhenko, Crystal chemistry and ab initio prediction of ultrahard rhombohedral B_2N_2 and BC_2N. *Solid State Sci.* **118** (2021) 106667.

[9] X. Luo, X. Guo, Z. Liu, J. He, D. Yu, Y. Tian, Ground-state properties and hardness of high density BC_6N phases originating from diamond structure. *J. Appl. Phys.* **101** (2007) 083505.

[10] Y. Gao, P. Ying, Y. Wu, S. Chen, M. Ma, L. Wang, Z. Zhao, D. Yu, First-principles studies of superhard BC_8N structures. *J. Appl. Phys.* **125** (2019) 175108.

[11] D.S. Scholl, J.A. Steckel, Density Functional Theory. A Practical Introduction (c) 2009 Wiley. ISBN: 13 978-0470373170.

[12] G. Kresse, J. Furthmüller, Efficient iterative schemes for ab initio total-energy calculations using a plane-wave basis set. *Phys. Rev. B* **54** (1996) 11169.

[13] G. Kresse, J. Joubert, From ultrasoft pseudopotentials to the projector augmented wave. *Phys. Rev. B* **59** (1999) 1758-1775.

[14] P.E. Blöchl, Projector augmented wave method. *Phys. Rev. B* **50** (1994) 17953-17979.

[15] J. Perdew, K. Burke, M. Ernzerhof, The Generalized Gradient Approximation made simple. *Phys. Rev. Lett.* **77** (1996) 3865-3868.

[16] W.H. Press, B.P. Flannery, S.A. Teukolsky, W.T. Vetterling, Numerical Recipes, 2nd ed. Cambridge University Press: New York, USA, 1986.

[17] P.E. Blöchl, O. Jepsen, O.K. Anderson, Improved tetrahedron method for Brillouin-zone integrations. *Phys. Rev. B* **49** (1994) 16223-16233.

[18] M. Methfessel, A.T. Paxton, High-precision sampling for Brillouin-zone integration in metals. *Phys. Rev. B* **40** (1989) 3616-3621.

[19] H.J. Monkhorst, J.D. Pack, Special k-points for Brillouin Zone integration. *Phys. Rev. B* **13** (1976) 5188-5192.

[20] A. Togo, I. Tanaka, First principles phonon calculations in materials science. *Scr. Mater.* **108**, (2015) 1-5.

[21] V. Eyert, Basic notions and applications of the augmented spherical wave method. *Int. J. Quantum Chem.* **77** (2000) 1007-1031.

[22] D. Fontaine, Structure du cyanure de sodium en phase ordonnée. *C. R. Acad. Sci. Série B* **281** (1975) 443-444.

[23] D. Williams, B. Pleune, K. Leinenweber, J. Kouvetakis, Synthesis and structural properties of the binary framework C–N compounds of Be, Mg, Al and Tl. *J. Solid State Chem.* **159** (2001) 244-250.

[24] A. Jain, S.P. Ong, G. Hautier, W. Chen, W.D. Richards, S. Dacek, S. Cholia, D. Gunter, D. Skinner, G .Ceder, K.A. Persson, Commentary: The Materials Project: A materials genome approach to accelerating materials innovation. *APL Mater.* **1** (2013) 011002.

[25] O. Reckeweg, C. Lind, A. Simon, F.J. DiSalvo, Synthesis, thermal and X-ray investigations of the high-temperature phase of copper(I) cyanide. *Z. Naturforsch. B* **58** (2003) 155-158

[26] M.J. Bucknum, R. Hoffmann, A hypothetical dense 3,4-connected carbon net and related B_2C and CN_2 nets built from 1,4-cyclohexadienoid units. *J. Am. Chem. Soc.* **116** (1994) 11456-11464.

[27] W. Voigt, Über die Beziehung zwischen den beiden Elasticitätsconstanten isotroper Körper. *Annal. Phys.* **274** (1889) 573-587.

[28] V.A. Mukhanov, O.O. Kurakevych, V.L. Solozhenko, The interrelation between hardness and compressibility of substances and their structure and thermodynamic properties. *J. Superhard Mater.* **30** (2008) 368-378.

[29] A.O. Lyakhov, A.R. Oganov, Evolutionary search for superhard materials: Methodology and applications to forms of carbon and TiO_2. *Phys. Rev. B* **84** (2011) 092103.

[30] X-Q. Chen, H. Niu, D. Li, Y. Li, Modeling hardness of polycrystalline materials and bulk metallic glasses. *Intermetallics*, **19** (2011) 1275-1281.

[31] E. Mazhnik, A.R. Oganov, A model of hardness and fracture toughness of solids. *J. Appl. Phys.* **126** (2019) 125109.

[32] V.A. Mukhanov, O.O. Kurakevych, V.L. Solozhenko, Thermodynamic aspects of materials' hardness: prediction of novel superhard high-pressure phases. *High Press. Res.* **28** (2008) 531-537.

[33] V.L. Solozhenko, Y. Le Godec, A hunt for ultrahard materials. *J. Appl. Phys.* **126** (2019) 230401

[34] Y. Le Godec, A. Courac, V.L. Solozhenko, High-pressure synthesis of superhard and ultrahard materials. *J. Appl. Phys.* **126** (2019) 151102.

[35] R.S. Krishnan, Raman spectrum of diamond. *Nature* **155** (1945) 171.

Table 1 Ternary B-C-N phases along with different types of model structure templates, space groups, numbers of formula units (Z), and energies (total, per formula unit and cohesive atom averaged; all in eV).

	Type	Space group (N)	Z	E_{tot}	E_{FU}	E_{coh}/at
BCN	*CoCN*	*R*3*m* (160)	3	-66.36	-22.12	-1.140
BCN	*CuCN*	*R*3*m* (160)	3	-67.92	-22.64	-1.313
BCN	*NaCN*	*Pmmn* (59)	2	-44.95	-22.97	-1.423
$B(CN)_3$	*Al(CN)₃*	*R*3*m* (160)	1	-54.98	-54.98	-1.341
C_6	*glitter*	$P4_2/mmc$ (131)	2	-51.82	-25.91	-2.037
BC_2	*glitter*	$P4_2/mmc$ (131)	2	-46.67	-23.34	-1.612
BCN	*glitter*	$P4_2mc$ (105)	2	-49.06	-24.53	-1.945
BC_2N [7]		*Pmm*2 (25)	1	-33.87	-33.87	-2.138
BC_2N [7]		*P*2221 (17)	2	-67.71	-33.85	-2.134

Atomic energies in eV: B (-5.3); C (-6.6); N (-6.8).

Table 2 Calculated crystal structures parameters

a) 'glitter' C_6, space group $P4_2/mmc$ (N° 131). (Fig. 2a)

a = 2.589 Å; c = 5.979 Å; V=40.076 Å^3; ρ = 2.984 g/cm^3

Atom	Wyckoff	x, y, z
C1	2*b*	½, ½, ¼
C2	4*c*	½, 0, 0.112

d(C2-C2) = 1.34 Å; d(C1-C2) = 1.536 Å
∠C2-C1-C2 =106.795°
∠C1-C2-C2 =122.517°

b) B_2C_4, space group $P4_2/mmc$ (N° 131) (Fig. 2b)

a = 2.667 Å; c = 6.480 Å; V=46.091 Å^3; ρ = 2.509 g/cm^3

Atom	Wyckoff	x, y, z
B	2*f*	½, ½, ¼
C	4*i*	½, 0, 0.104

d(C-C) = 1.35 Å; d(B-C) = 1.634 Å
∠C-B-C = 109.532°
∠C-C-B = 125.32°

c) $B_2C_2N_2$, space group $P4_2mc$ (N° 105) (Fig. 2c)

a = 2.705 Å; c= 6.006 Å; V=43.902 Å^3; ρ = 2.783 g/cm^3

Atom	Wyckoff	x, y, z
B	2*b*	½, ½, 0.2511
C	2*c*	½, 0, 0.1076
N	2*c*	½, 0, 0.8913

d(C-N) = 1.29 Å; d(B-C) = 1.817 Å; d(B-N) = 1.593 Å
∠N-B-N = 116.21°
∠C-B-C = 114.96°

Table 3 Calculated elastic constants and resulting bulk (B_V) and shear (G_V) moduli (in GPa)

	C_{11}	C_{12}	C_{13}	C_{33}	C_{44}	C_{66}	B_V	G_V
C_6	715	45	95	1172	69	75	341	283
B_2C_4	478	74	106	861	62	80	249	206
$B_2C_2N_2$	569	74	114	932	63	88	280	232

Table 4 Mechanical properties: Vickers hardness (H_V), bulk modulus (B), shear modulus (G), Young's modulus (E), Poisson's ratio (ν) and fracture toughness (K_{Ic})

	H_V			B		G_V	E [§]	ν [§]	K_{Ic} [**]
	T[*]	LO[†]	CN[‡]	B_0 [*]	B_V				
	GPa								MPa·m$^{1/2}$
C_6	83	75	41	376	341	283	665	0.175	5.6
B_2C_4	53	49	33	255	249	206	484	0.176	3.6
$B_2C_2N_2$	65	61	36	282	280	232	545	0.175	4.2

[*] Thermodynamic model [28]

[†] Lyakhov-Oganov model [29]

[‡] Chen-Niu model [30]

[§] E and ν values calculated using isotropic approximation

[**] Mazhnik-Oganov model [31]

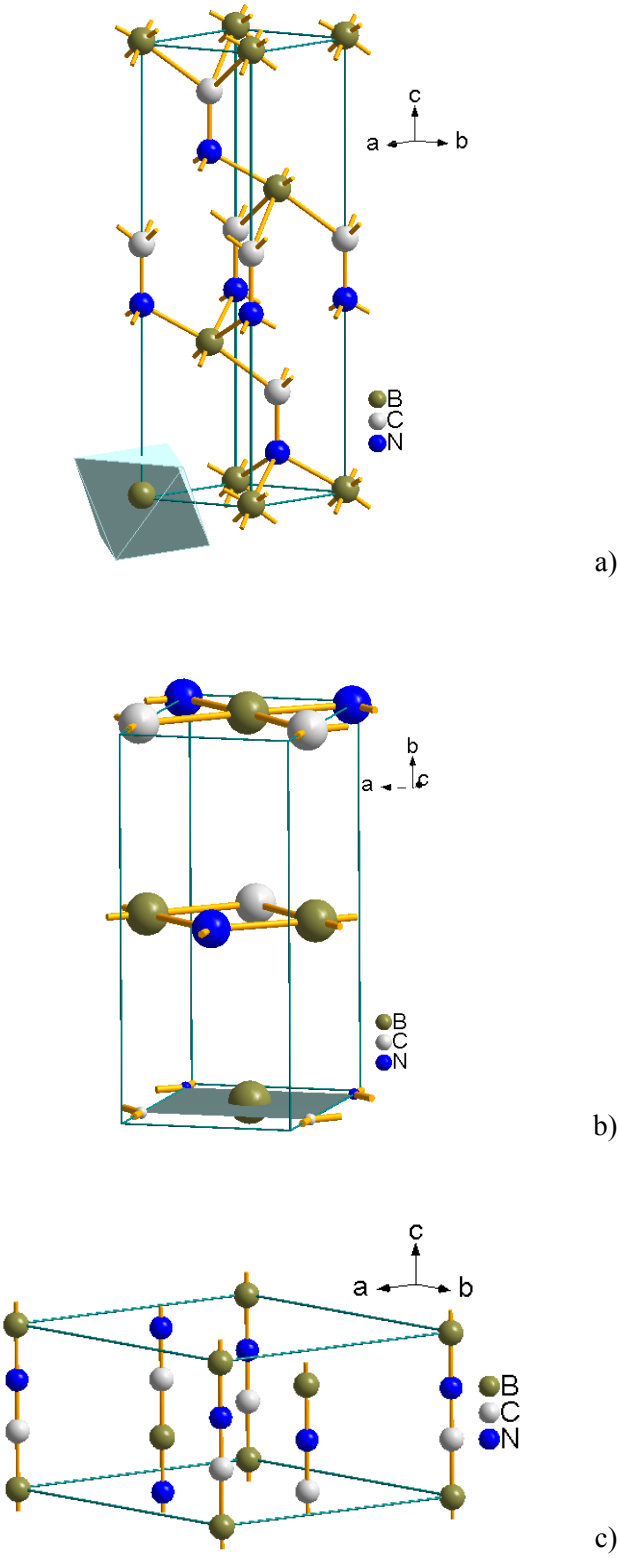

Figure 1 BCN structures calculated in preliminary steps using three templates highlighting different spatial coordination of boron (cf. Table 1): a) rhombohedral CoCN-like; b) orthorhombic NaCN-like and c) rhombohedral CuCN-like.

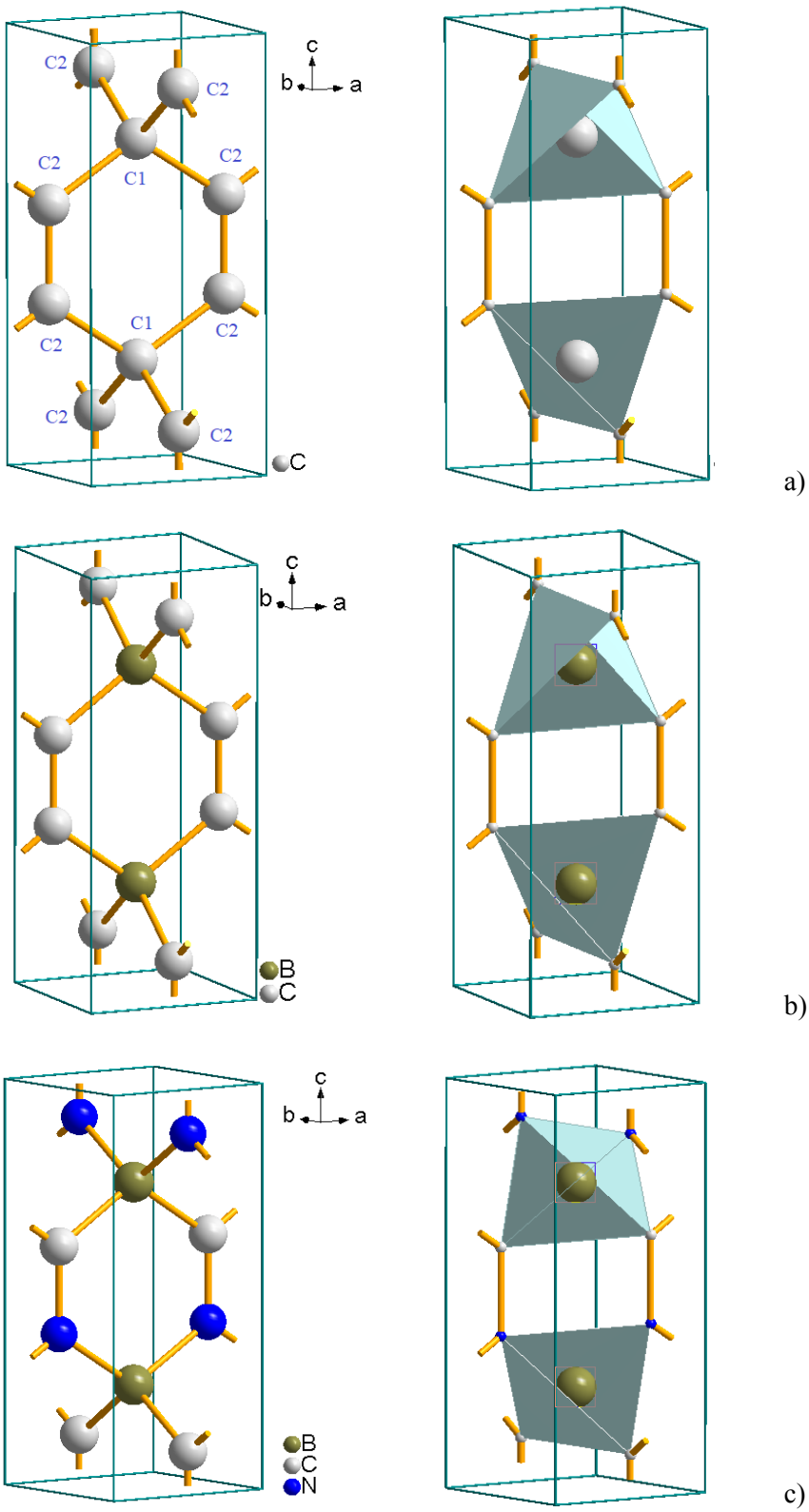

Figure 2 Sketches of tetragonal structures with coordination polyhedra projections. a) 'glitter' C_6 with two different kinds of carbon (tetrahedral C1 & trigonal C2) and b) 'glitter'-based B_2C_4 (both with space group $P4_2/mmc$); and c) equiatomic $B_2C_2N_2$ (space group $P4_2mc$). Olive, grey and blue spheres correspond to B, C and N atoms, respectively.

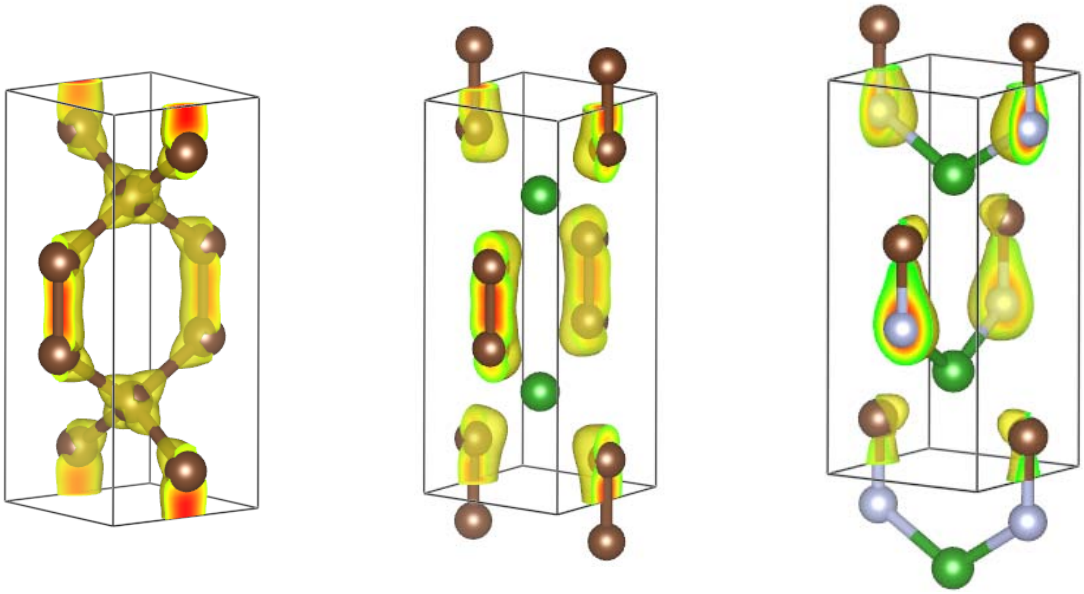

a) b) c)

Figure 3 Charge density projections (yellow volumes on and between atoms). a) 'glitter' C_6, b) 'glitter'-based B_2C_4, c) $B_2C_2N_2$. Green, grey and brown spheres correspond to B, N and C atoms, respectively.

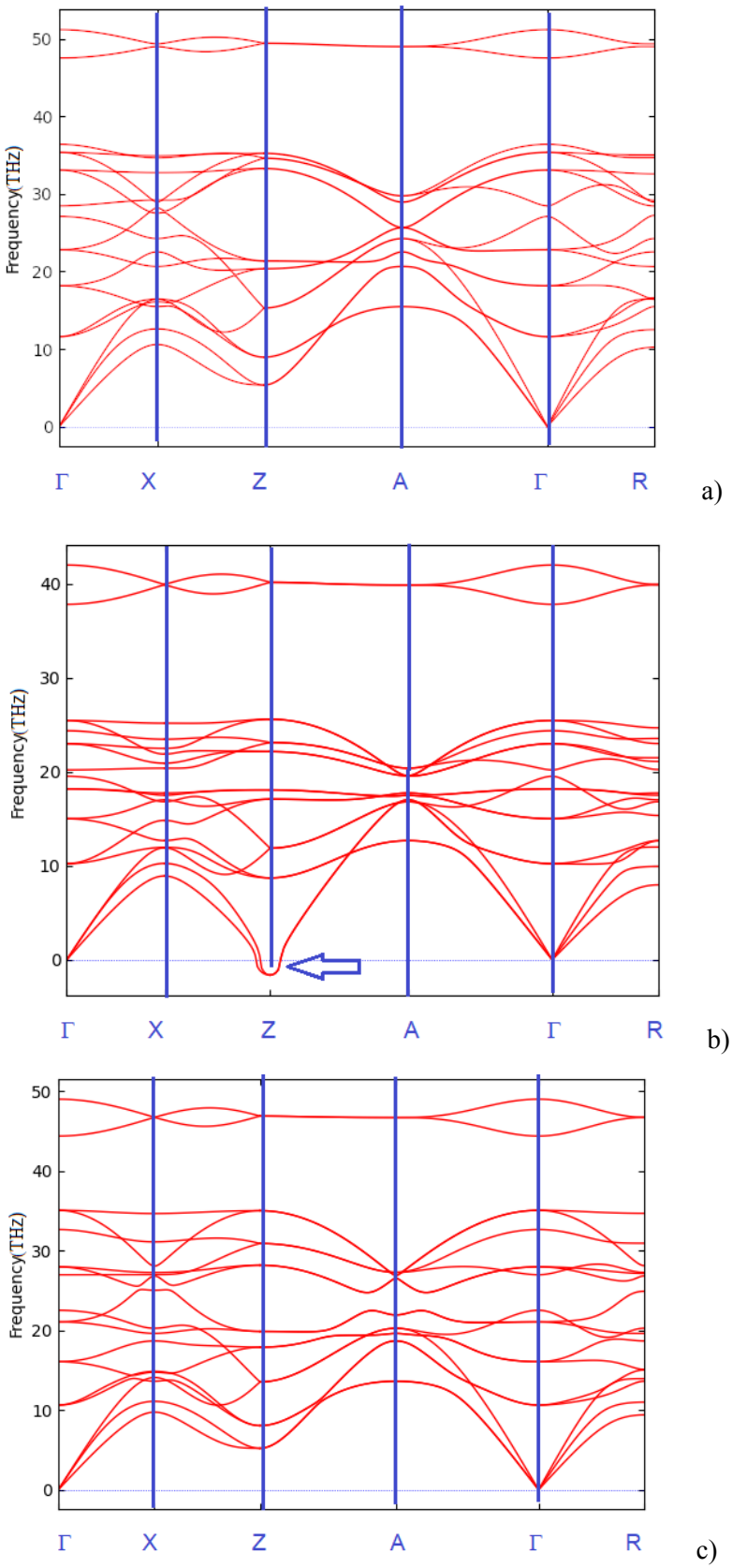

Figure 4. Phonon band structures along tetragonal Brillouin zone directions. a) 'glitter' C_6, b) 'glitter'-based B_2C_4, c) $B_2C_2N_2$.

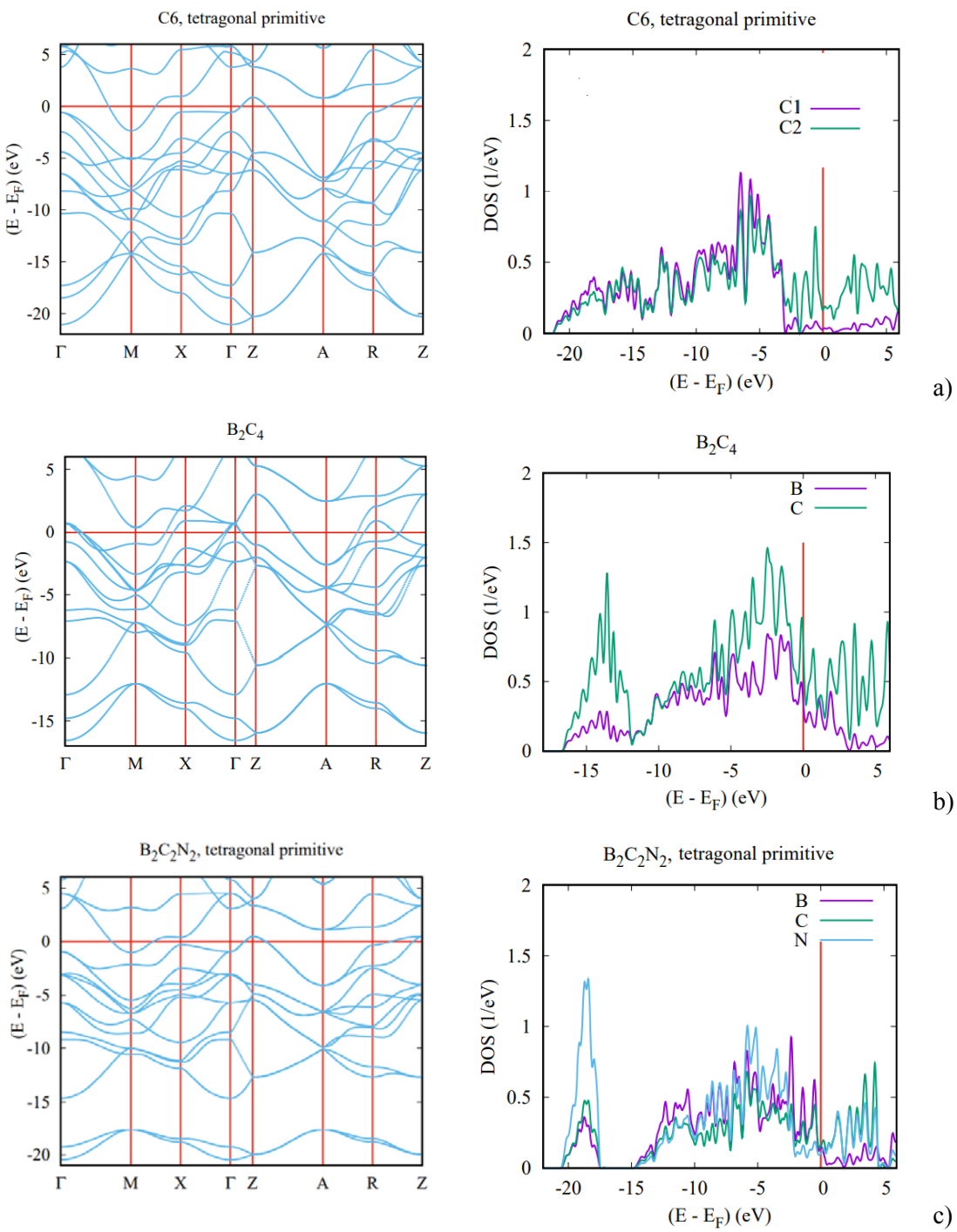

Figure 5 Electronic band structures and site projected density of states: a) 'glitter' C_6, b) 'glitter'-based B_2C_4, c) $B_2C_2N_2$.